

CALYPSO structure prediction method and its wide application



Hui Wang^a, Yanchao Wang^{a,b}, Jian Lv^{a,c}, Quan Li^{a,b}, Lijun Zhang^{a,b}, Yanming Ma^{a,*}

^a State Key Laboratory of Superhard Materials, Jilin University, Changchun 130012, People's Republic of China

^b College of Materials Science and Engineering, Jilin University, Changchun 130012, People's Republic of China

^c Beijing Computational Science Research Center, Beijing 100084, People's Republic of China

ARTICLE INFO

Article history:

Received 15 June 2015

Accepted 15 September 2015

Available online 19 October 2015

Keywords:

Structure prediction

Swarm-intelligence algorithm

First principles

ABSTRACT

Atomistic structure prediction from “scratch” is one of the central issues in physical, chemical, materials and planetary science, and it will inevitably play a critical role in accelerating materials discovery. Along this thrust, CALYPSO structure prediction method by taking advantage of structure smart learning in a swarm was recently developed in Prof. Yanming Ma's group, and it has been demonstrated through a wide range of applications to be highly efficient on searching ground state or metastable structures of materials with only the given knowledge of chemical composition. The purpose of this paper is to provide an overview of the basic theory and main features of the CALYPSO method, as well as its versatile applications (limited only to a few works done in Ma's group) on design of a broad range of materials including those of isolated clusters/nanoparticles, two-dimensional reconstructed surfaces, and three-dimensional bulks (at ambient or high pressure conditions) with a variety of functional properties. It is to say that CALYPSO has become a major structure prediction technique in the field, with which the door for a functionality-driven design of materials is now opened up.

© 2015 Elsevier B.V. All rights reserved.

1. Introduction

There is a growing need for efficient methods to predict materials' atomic structures. In recent years, first principles methods have been widely used in materials science. Such approaches apply quantum mechanics and statistical mechanics to the structural information of a material to simulate with acceptable accuracy many of its macroscopic physical properties [1]. However, a lack of suitable structural information can lead the predicted properties to diverge permanently away from those experimentally measured. Therefore, structure prediction methods that could inform which atomic configuration of a material usually exists experimentally are greatly needed to accelerate the discovery of useful new materials.

Structure prediction involves exploring the potential energy surface (PES), which gives the energy of a structure as a function of its atomic coordination. The PES can be regarded as a multi-dimensional system consisting of many hills and valleys connected by saddle points. A local minimum (i.e., the lowest point in a valley) gives a stable structure. The global minimum of the PES represents the ground-state structure. An experimentally synthesizable material should have the ground state structure if which is kinetically accessible; therefore, the global minimum is the target of structure

prediction. It is not difficult to predict the ground-state structure for a small system of several atoms, as all the local minima on the PES are generally obtainable by local structure optimizations starting from a number of guessed structures [2]. In this case, the global minimum can be determined in one shot; however, the challenge of structure prediction increases significantly with increasing complexity of the PES. For large systems with tens or hundreds of atoms, the ground-state structure might hide among very many stable structures. Consequently, finding the ground-state structure would require global optimization methods to greatly improve the efficiency and success rate of structure prediction.

In the past decade, much effort has been devoted to structure prediction. Several advanced methods have been developed [3–16] and these methods have led to many exciting discoveries that have been examined in several reviews (e.g., Refs. [17–21] and references therein). We have recently developed an efficient CALYPSO (Crystal structure ANALysis by Particle Swarm Optimization) method [22–27] on structure prediction from “scratch”. Here we focus on CALYPSO methodology and its application to structural design on some typical material systems.

2. CALYPSO methodology for structure prediction

CALYPSO is a global optimization algorithm for crystal structure prediction. Its efficiency derives from the successful integration of

* Corresponding author.

E-mail addresses: huiwang@jlu.edu.cn (H. Wang), mym@jlu.edu.cn (Y. Ma).

several major techniques that are critical for PES exploration. These are: (i) structural evolution through a swarm-intelligence algorithm for driving the search to deep valleys on the PES; (ii) structural characterization techniques to avoid duplicated searching of equivalent regions of the PES; (iii) symmetry constraints during structure generation and local optimization to reduce the searching space; and (iv) local structural optimization to find local minima on the PES.

2.1. Swarm-intelligence algorithm

Our CALYPSO method adopts a “self-improving” strategy to locate the global minimum of the PES via particle swarm optimization (PSO) [28]. The PSO algorithm is a typical swarm-intelligence scheme [29] inspired by natural biological systems (e.g., ants, bees, or birds), and has been applied to a variety of fields in engineering and chemical science [30]. The application of PSO algorithm in structure prediction started only recently [31]. Within the CALYPSO method, structures are evolved in the energy landscape through velocity according to formula (1). The new velocity of each structure (v^{t+1}) is calculated by Eq. (2) using the properties of itself and of the global population. The calculation includes the structure’s previous location (x^t) before optimization, previous velocity (v^t), and current location ($pbest^t$) with an achieved best fit (i.e., the lowest enthalpy) of the individual structure. The population global location ($gbest^t$) with the best fit for the entire population is also considered.

$$x^{t+1} = x^t + v^{t+1} \quad (1)$$

$$v^{t+1} = \omega v^t + c_1 r_1 (pbest^t - x^t) + c_2 r_2 (gbest^t - x^t) \quad (2)$$

where w denotes the inertia weight, which is dynamically varied and decreases linearly from 0.9 to 0.4 during the iteration; c_1 and c_2 are the self-confidence factor and swarm confidence factor, respectively; and r_1 and r_2 are random numbers distributed in the range [0, 1]. The random parameters r_1 and r_2 ensure good coverage of the searching space, and avoid entrapment in local minima. The strong ability of PSO to overcome large barriers in energy landscapes derives from the use of swarm intelligence.

Two versions of the PSO method (one local and one global) have been implemented in CALYPSO [22–27]. The global PSO, outlined in Fig. 1(a), has only one global best structure acting as the attractor for the entire structure population, and all particles seek new positions only in the regions close to the uniquely overall best position. This method converges quickly for small systems (i.e., those with fewer than 30 atoms in the simulation cell), but it may be less effective for larger systems containing more than 30 atoms per

simulation cell, because the PES becomes much more complex. The local PSO is outlined in Fig. 1(b). Each particle (i.e., a candidate structure) selects a set of other particles as its neighbors, and its velocity is adjusted according to both its position and the best position achieved so far in the community formed by its neighborhood. Thus, at each iteration the particle will move toward its own best position and the best position of its local neighborhood, rather than the overall best position in the swarm. By maintaining multiple attractors that lead to the formation of different structural motifs, the local PSO allows an unbiased and efficient exploration of large space on the PES, thus effectively avoiding premature convergence during structure searches.

2.2. Fingerprinting structures via a bond characterization matrix

Structure evolution is hindered by similar nearby structures in the same valley of the PES. It is challenging to remove similar structures to enhance the structural diversity and also to avoid wasting computational efforts during structure evolution. Assessing similarities among structures requires fingerprinting them based on their complete geometric information (i.e., bond lengths and angles). Our developed structural characterization technique, the bond characterization matrix (BCM), is based on bond lengths and angles, and is implemented in our CALYPSO method. BCM is realized by constructing a set of modified bond-orientational order metrics [32] for structure quantification, where spherical harmonic and exponential functions are used to characterize the bond angles and lengths, respectively. Specifically, for a given structure, a bond vector \vec{r}_{ij} between atoms i and j is defined if the interatomic distance is less than a given cutoff distance. This vector is associated with the spherical harmonics $Y_{lm}(\theta_{ij}, \phi_{ij})$, where θ_{ij} and ϕ_{ij} are the polar angles, and where the weighted average over all bonds formed by, for instance, the A and B atoms can be derived as follows:

$$\bar{Q}_{lm}^{\delta_{AB}} = \frac{1}{N_{\delta_{AB}}} \sum_{i \in A, j \in B} e^{-\alpha(r_{ij} - b_{AB})} Y_{lm}(\theta_{ij}, \phi_{ij}), \quad (3)$$

where δ_{AB} and $N_{\delta_{AB}}$ denote the type and the number of bonds, respectively. Only even- l spherical harmonics are used in Eq. (3) to guarantee invariant bond information with respect to the direction of the bonds. To avoid dependence on the choice of reference frame, it is important to consider the rotationally invariant combinations [32],

$$Q_l^{\delta_{AB}} = \sqrt{\frac{4\pi}{2l+1}} \sum_{m=-l}^l |\bar{Q}_{lm}^{\delta_{AB}}|^2, \quad (4)$$

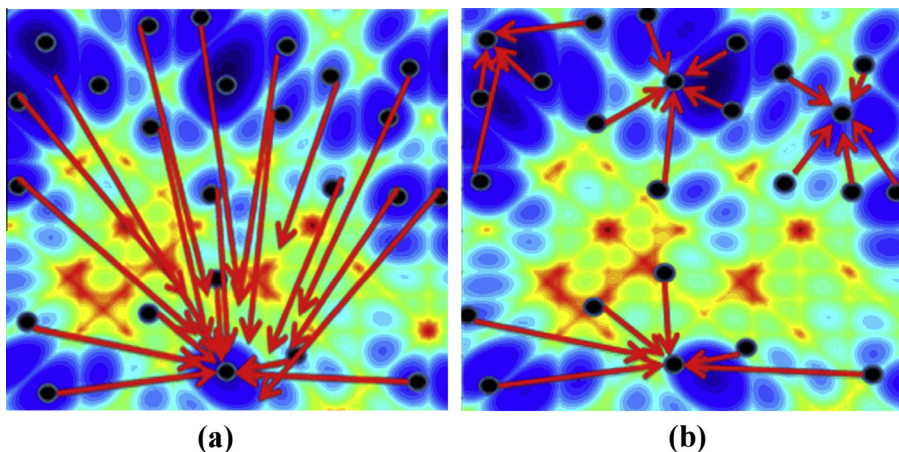


Fig. 1. The schematic diagram of global (a) and local (b) PSO.

where each series of $Q_l^{\delta_{AB}}$ for $l = 0, 2, 4, 6, 8, 10$ can be used to represent a type of bond, and is thus an element of the BCM. By including the complete structural information of bond lengths and angles, this technique provides unambiguous fingerprinting for structures. As a result, the similarity of two structures can be quantitatively evaluated by the Euclidean distance between their BCMs:

$$D_{uv} = \sqrt{\frac{1}{N_{\text{type}}} \sum_{\delta_{AB}} \sum_l (Q_l^{\delta_{AB},u} - Q_l^{\delta_{AB},v})^2}, \quad (5)$$

where u and v denote two individual structures, and N_{type} is the number of bond types. Currently, the BCM technique has been applied to the structure prediction of 3D crystals [23] and 0D clusters [24].

2.3. Structure generation with symmetry constraints

The structure of an ordered material is governed by symmetry rules. Symmetry constraints in structure generation and in local optimization preclude the appearance of disordered structures, reduce the searching space of the PES, and improve the efficiency of local structural optimizations. Consequently, symmetry constraints for structure generation are implemented in our CALYPSO method. Different strategies for dealing with 0D-isolated systems, 2D layers or surfaces, and 3D crystals are designed to generate random symmetric structures. In particular, the generation of random structures is constrained by the 32 point groups for isolated systems (e.g., molecules, clusters, and nanoparticles), the 17 in-plane space groups for 2D layers or surfaces, and the 230 space groups for bulk crystals.

2.4. Local structural optimization

The PES of a material can be regarded as a multi-dimensional system of many hills and valleys connected by saddle points. Given that the global minimum is one of the possibly many local minima, local searching is an inevitable part of the global search, and therefore should be included in any efficient structure searching method. The CALYPSO method currently has interfaces with various *ab initio*- and force-field-based total-energy packages (e.g., VASP [33], SIESTA [34], Quantum-Espresso [35], CASTEP [36], CP2K [37], Gaussian [38], DFTB+ [39], LAMMPS [40], and GULP [41]) for local structural optimization. Other external total-energy programs can also be easily interfaced with CALYPSO as required.

3. Features

CALYPSO currently implements many features to solve effectively various structure prediction problems, which can include: (i) searching for the energetically stable/metastable structures of a given chemical composition for most materials ranging from 0D to 3D systems; (ii) conducting searches for automatically varying chemical compositions; and (iii) searching with partially fixed structural information.

3.1. Clusters or nanoparticles

Clusters are nano-objects composed of a few to several thousand atoms or molecules. As 0D non-periodic systems, they can be constructed following point group symmetry, and CALYPSO can be used in the structure searching of such 0D systems [24]. Although an infinite number of point groups can be utilized for structure generation, we found that the use of a small number of simple point groups can effectively improve the sampling of the PES. The current version of CALYPSO generates structures by utilizing common point groups in molecules. Energy evaluation

with periodic boundary conditions employs a supercell model (Fig. 2(a)) with the cluster at the center surrounded by a vacuum large enough to prevent interaction between the cluster and its periodic images. Here, Cartesian coordinates are used straightforwardly for structure representation and for evolution by PSO. The module for cluster structure searching has been extensively benchmarked in Lennard–Jones cluster systems of varied size (up to 150 atoms), and high search efficiency has been achieved [24].

3.2. Layer structures

CALYPSO can implement a 2D structure search module to predict the structures of 2D layered materials (e.g., planar monolayer, buckled monolayer, and multiple layers) [25]. The models for 2D layer structure simulations using CALYPSO are illustrated in Fig. 2(b); the supercell contains a layered material part and a vacuum part. The atoms in the layered material part are fully evolved and optimized during structure search, while the vacuum region is used to ensure that the studied layer materials are isolated from their nearest-neighboring periodic images. Note that a distortion parameter perpendicular to the in-plane layer (Δz in Fig. 2(b)) and a van der Waals gap parameter (i.e., the distance between two adjacent layers) should be introduced for predicting the structures of buckled layer and multi-layered systems. The module of 2D layer structure prediction has been extensively benchmarked in graphene, hexagonal BN, and some quasi-2D group 6 metals chalcogenides.

3.3. Surface reconstructions

To search the structures of surfaces, CALYPSO adopts a slab model [26]. In particular, a supercell model containing slabs separated by a vacuum along the direction perpendicular to the surface (Fig. 3(a)) is used to simulate the surface structure. The slab consists of three regions: the bulk material region, the unreconstructed surface, and the reconstructed surface. The bulk region is fixed to preserve the bulk nature of the material, while the atoms in the unreconstructed surface region are subject to local structural relaxation, but are not involved in the structural evolution. Only atoms in the reconstructed surface region are fully evolved during structure searching. The fitness function during structural evolution is set to the surface excess free energy, which represents the energetic stability of the surface reconstructions, as follows:

$$\Delta\gamma(\mu) = \frac{1}{A} \left(E_{\text{surf}}^{\text{tot}} - E_{\text{ideal}}^{\text{tot}} - \sum_i n_i * \mu_i \right), \quad (6)$$

where A is the area of the studied surface (usually in the unit of a 1×1 planar unit cell), $E_{\text{surf}}^{\text{tot}}$ represents the total energy of the surface (with the subscripts *surf* and *ideal* representing the reconstructed and the ideal unreconstructed surfaces, respectively), and n_i and μ_i are the number and chemical potential of the i th type species in the surface region, respectively.

3.4. Crystals

A crystal structure can be defined by two types of variables: lattice parameters (the lengths of three lattice vectors and the three angles among them) and atomic fractional coordinates (three components coded as the fractions of lattice vectors for each atom). To achieve the global minimum on the PES, these variables are evolved simultaneously in both the structure evolution through the swarm-intelligence algorithm and the local structural optimization. Note that crystal structure prediction at high pressure can be realized easily by fixing the pressure condition in the local structure optimization. In high-pressure investigations, the CALYPSO method

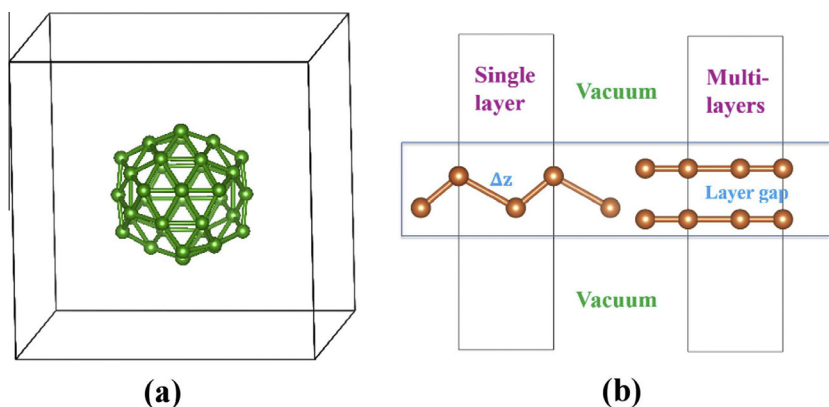


Fig. 2. The models used in CALYPSO for cluster structure (a), single and multi-layer structure (b).

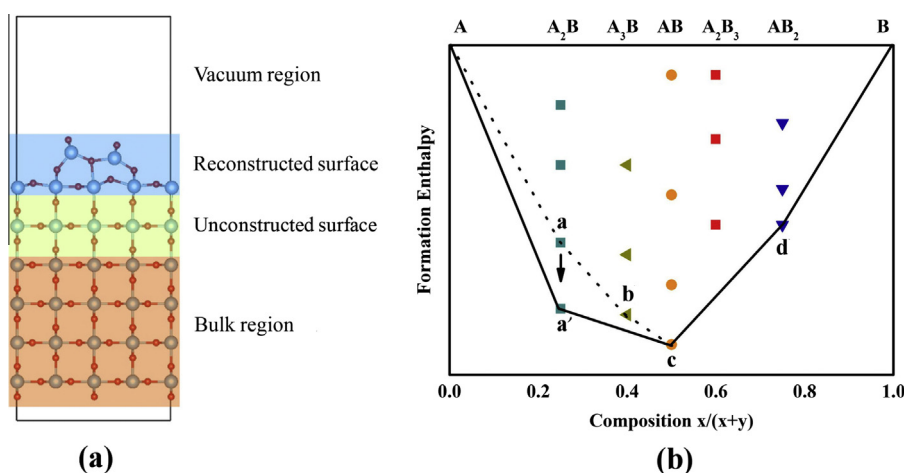


Fig. 3. The models used in CALYPSO for surface reconstruction structure (a) and the illustration of the evolution of convex hull in structure prediction for automatic variation of chemical compositions (b).

[22,23] can take advantage of known pressure–volume relations by accordingly initializing the volume of the simulation cell.

3.5. Structural constraints

Partial structural information (e.g., the unit cell, partial atomic positions, molecular unit, or structural motif) is sometimes available from experiments. Taking full advantage of such information is extremely useful for structure searching, because it can significantly reduce the configuration space of candidate structures. For this we have implemented a module in CALYPSO that can flexibly use any known partial structural information. For example, in a system with the molecular unit experimentally known, the Z-matrix method [42] is employed to represent the rigid molecular unit, which can only move or rotate as a whole unit during structural evolution. Other prior structural knowledge such as lattice parameters, partial atomic positions, or space group can also be used to accelerate structure searching, and thus ensure that the search proceeds in the right direction.

3.6. Variable compositions

To identify all the energetically stable structures throughout the whole composition range in one process, CALYPSO implements a module for the automatic variation of chemical compositions for structure searching. This module can construct a full convex hull of formation energy vs. composition for a given system. The

evolution of the convex hull during the structure search is illustrated in Fig. 3(b): at the n th step, the available lowest-energy structures (i.e., a–d) at different stoichiometries are used to construct an approximate convex hull. Subsequently, the new convex hull is updated by considering the newly emerged structure, leading to the formation of a new hull through c and d at the $(n + 1)$ th step. The structure b is reasonably discarded as its formation energy lies above the tie line between the neighboring pair of structures a' and c. A direct search for the convex hull using this module is usually more efficient than a study involving separate structure searches at different compositions.

4. Applications

The CALYPSO method has been widely used to investigate materials ranging from 0D clusters to 3D crystals by searching the energetically stable/metastable structures at given chemical compositions. It has made some exciting discoveries that have been confirmed experimentally; e.g., high-pressure semiconducting Aba_2-40 phase of elemental lithium, high-temperature superconductivity in sulfur hydrides [43], and the two long-puzzling high-pressure superconducting phases of bismuth telluride [44]. Here we focus on a few recent applications of CALYPSO by our group that include the discovery of several novel materials such as nanoclusters, a diamond surface, superhard materials, energetic materials, electrides, superconductors, and materials in the Earth's core, etc.

4.1. Nanoclusters

Clusters, the basic building blocks of nanomaterials, exhibit structural and electronic properties with intriguing size- and composition-dependent behaviors. If specific clusters with chemical properties that resemble atoms can be produced, they can be regarded as man-made superatoms. Subsequent assembly of these superatoms may lead to materials with novel properties. By means of the CALYPSO cluster structure prediction method [24], we have performed structure searches for medium-sized boron [45] and transition-metal-doped boron clusters [46] in an effort to design boron fullerene-type clusters.

The discovery of the C_{60} allotrope [47] opened the new field of fullerene research. The associated search for fullerene-like structures formed by elements other than carbon has become one of the most challenging tasks facing the physical, chemical, and material sciences. Boron, a neighbor of carbon in the periodic table, can adopt sp^2 and sp^3 bonding similar to carbon, and thus is a promising candidate for forming fullerene-like structures. We recently used CALYPSO to predict a B_{38} fullerene analogue [45]. Its structure (Fig. 4(a)) is highly symmetric and consists of 56 triangles and four hexagons, which provide an optimal void in the center of the cage. Energetically, it is more favorable than the planar and tubular structures, and it possesses an unusually high chemical stability: a large energy gap (~ 2.25 eV) and a high double aromaticity, superior to those of most aromatic quasi-planar B_{12} and double-ring B_{20} clusters. Our findings represent a key step toward understanding the structures of medium-sized B clusters and the discovery of the direction of experimental synthesis of all-boron fullerene analogues. Soon after the prediction of B_{38} fullerene, B_{40} fullerene have been observed through a joint theoretical and experimental work [48], and the B_{39} fullerene with axially chiral feature is subsequently identified by Chen et al. [49]. These results imply that the transition to fullerene-like B_n clusters occurs around transition demarcation $n \sim 38$.

Inspiring by the well-documented metallofullerenes [50] and endohedral doped silicon fullerenes [51–53], it is of current interest to access the possibility of stabilization smaller boron fullerene through transition metal encapsulation. Thus, we have systematically investigated structural stabilities of the B_{24} clusters doped by a series of transition metals including Ti, Zr, Hf, Cr, Mo, W, Fe, Ru and Os [46]. We find that the free energy landscapes of B_{24} clusters are qualitatively changed after transition metal atoms encapsulated, where the cage-like rather than originally quasi-planar structures emerge as energetically favorable isomers. Most strikingly, while in most of cases the stable endohedral cage processes

low symmetry, a high-symmetry $D3h$ cage is stabilized by Mo/W encapsulation. Further analysis indicates that the endohedral $D3h$ cage exhibits robust thermodynamic, dynamical and chemical stabilities. The physical mechanism responsible for the stabilities is attributed to their unique electronic structure of 18-electron closed-shell configuration.

4.2. Diamond surface

The diamond (111) and (100) surfaces are of both fundamental and technical interest. It is theoretically interesting to understand the forces driving reconstruction and bonding, especially when the diamond surfaces are compared with those of other group 14 semiconductors (i.e., silicon and germanium) [54–56]. Practical uses of the diamond (100) and (111) surfaces arise from their being the two dominant growth planes in the production of diamond by chemical vapor deposition [57].

We used the CALYPSO surface reconstruction search method [26] to identify a hitherto unexpected surface reconstruction of diamond (100). The structure contains a self-assembly of carbon nanotube (CNT) arrays (Fig. 4(b)). Our calculations indicate that the surface with self-assembled CNTs is energetically degenerate to the dimer structure under normal conditions, but becomes much more favorable under a small compressive strain or at elevated temperatures. The intriguing covalent bonding between neighboring tubes creates a unique feature of carrier kinetics that has one dimensionality of the hole states but two dimensionality of the electron states. This might lead to new materials with superior electronic properties. Our findings highlight that the surface plays a vital role in the fabrication of nanodevices by being a functional part of them [26].

4.3. Superhard materials

The mechanical properties of superhard materials (hardness above 40 GPa) lend them to wide industrial use as cutting, polishing, and drilling tools, and as surface-protecting coatings. Crystals with three-dimensional covalent bonds formed by light elements or light elements and transition metals have high resistance against elastic deformation, and are therefore preferred targets in the search for novel superhard materials. We developed a methodology [27] for the efficient design of new superhard materials that requires only the chemical compositions and certain external conditions. It uses hardness as fitness function during structure evolution and constructs a hardness vs. energy map from which the energetically favorable superhard or hard structures are readily

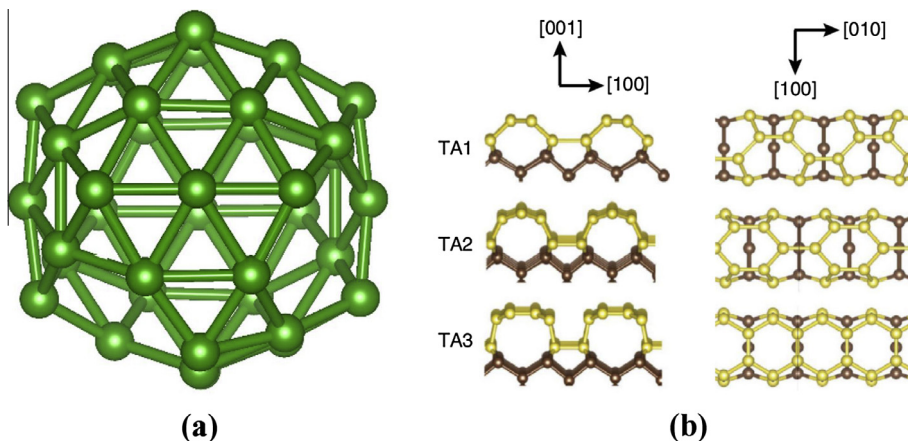


Fig. 4. The structures of (a) B_{38} , (b) three types of diamond nanotube-array reconstruction.

accessible. The identified structures are important candidates for further theoretical or experimental exploration. Here we present several applications of the CALYPSO algorithm to the design of superhard materials for technically important systems [58–63].

Recently, a new cubic BC_3 (c- BC_3) phase was synthesized by the direct transformation of graphitic BC_3 at 39 GPa and 2200 K [64]. However, the lack of an accurate structural determination impedes further understanding and exploration of these novel BC compounds, and calls for an innovative approach to solving such complex crystal structures. We have identified a BC_3 phase in the cubic diamond structure by using the CALYPSO crystal structure prediction method. It contains a distinct boron bonding network along the body diagonals of its 64-atom unit cell (Fig. 5(a)) [58]. This new structure conforms to the experimental constraints on the cubic crystal symmetry and all- sp^3 -type bonding, and its simulated X-ray diffraction and Raman spectra almost perfectly match the experimental data. The highly symmetric boron bonding network plays an important role in stabilizing the cubic diamond structure. Calculated stress–strain relations reveal its intrinsic superhard nature combined with a superior ductility driven by intriguing sequential bond-breaking processes that do not exist in diamond or c-BN. These results establish the first cubic diamond phase in a boron carbide, and indicate its remarkable structural properties. This work serves as an exemplary case study of strong covalent solids with complex bonding configurations, and the insights gained here may help to explore other complex binary and ternary covalent compounds.

The synthesis of boron-rich tungsten borides has reignited great interest in these compounds, which show outstanding properties (e.g., ultra hardness, high melting points, and strong resistance to oxidation and acids) that rival or exceed those of traditional superhard materials. Detailed understanding of these compounds, however, has been impeded by uncertainties regarding their complex crystal structures. We have performed a systematic global structural optimization of tungsten borides using CALYPSO, and

identified the thermodynamically stable structures as well as a large number of metastable structures over a wide range of boron concentrations [59]. On the basis of the calculated convex hull, we predict that $P6_3/mmc$ -2u WB_2 , $R\bar{3}m$ -6u WB_3 , and $P6_3/mmc$ -2u WB_4 are thermodynamically stable and thus viable for experimental synthesis. Comparing the experimental and simulated X-ray diffraction patterns leads to the identification of previously synthesized $I4/m\bar{4}u$ W_2B , $I4_1/amd$ -8u WB , $P6_3/mmc$ -4u WB_2 , and $P6_3/mmc$ -4u WB_3 . These results clarify and correct previous structural assignments as well as provide a blueprint for analyzing a variety of tungsten borides. They therefore have broad implications for the further exploration of this class of promising materials. Our results are also expected to stimulate new material exploration and discovery, and our method is applicable to exploring the rich and complex structures of other compounds of transition metals and light elements.

4.4. Energetic materials

Covalently bonded extended phases of molecular solids comprising first- and second-row elements at high pressures are potential high-energy-density materials (HEDMs) [65]. The existence of such extended solids has recently been demonstrated using diamond anvil cells in several systems, including nitrogen [66] and carbon monoxide [67]. We used CALYPSO [22] to propose the ground-state structures of several HEDMs at high pressures [68–70].

It has been reported that triply bonded molecular nitrogen dissociates into singly bonded polymeric nitrogen under high pressure [66]. The exploration of stable high-pressure forms of polymeric solid nitrogen is of great interest. We used CALYPSO to explore the high-pressure phases of solid nitrogen, and thus discovered a hitherto unexpected cage-like diamondoid structure of polymeric nitrogen [68]. The structure (Fig 5(b)) adopts a highly symmetric body-centered cubic structure with lattice sites occupied by diamondoids, each of which consists of 10 nitrogen atoms

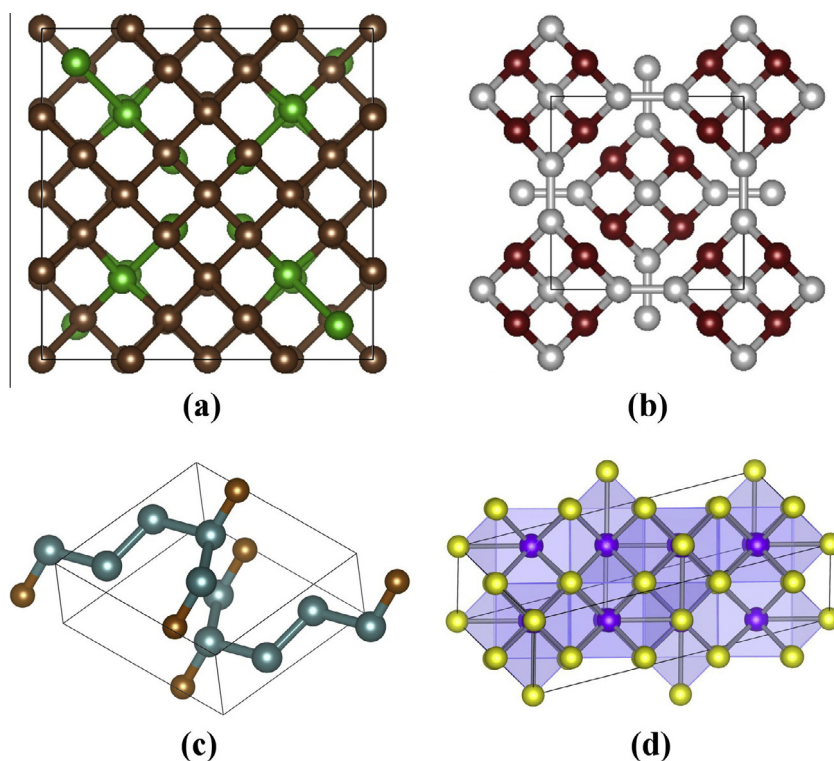


Fig. 5. The crystal structures: (a) B38, (b) the diamondoid structure of polymeric nitrogen, (c) P-1 structure of N_2H , and (d) the disordered bcc structure Bi_2Te_3 .

that form a tetracyclic cage. This prediction provides an unexpected example of a structure created by the compression of a molecular solid, and represents a significant step toward understanding the behavior of solid nitrogen and other nitrogen-related materials under extreme conditions.

Hydronitrogen represents a rich family of nitrogen-containing materials; their extremely high mass ratio of nitrogen makes them particularly attractive for HEDMs. Under ambient conditions, ground-state hydronitrogen adopts an ammonia phase consisting of NH_3 molecules. Under certain conditions some metastable phases can be synthesized, including hydrazine (N_2H_4), diazene (N_2H_2), ammonium azide (NH_4N_3), and tetrazene (N_4H_4) [69]. The diversity of these metastable phases indicates the versatile capability of hydrogen in stabilizing a wide range of compounds with low-order N–N bonds. We used CALYPSO to perform a comprehensive crystal structure search for energetically stable hydronitrogen phases with varied H and N contents up to 200 GPa [69], and found a previously unknown polymeric N_2H phase of hydronitrogen (Fig. 5(c)). This phase is energetically stable against decomposition above a relatively low pressure of ~ 33 GPa; it consists of a polymeric framework of infinite armchair-like nitrogen chains, and shows novel metallic features caused by the charge-transfer process and the delocalization of p electrons within the quasi-one-dimensional nitrogen chains. Its expectedly high energy density of ~ 4.40 kJ/g originates from the alternate N–N single and double bonds in the infinite nitrogen chains.

4.5. Substitutional alloy

Alloys can show physical properties superior to those of each individual component, and are widely used in engineering and industry. A common type of alloy is the substitutional crystalline solid solution, in which atoms of one element randomly substitute for atoms of another element. The search for new substitutional alloys is a central theme in a broad range of scientific disciplines.

A well-known thermoelectric material and a topological insulator, Bi_2Te_3 crystallizes in the rhombohedral $R\bar{3}m$ structure under ambient conditions [71]. Under pressure, it transforms into several superconducting phases whose structures have been left unsolved for decades [72]. We used CALYPSO for crystal structure prediction to solve the two long-puzzling low/high-pressure superconducting phases as seven- and eightfold monoclinic structures, respectively [44]. We experimentally found that above 14.4 GPa, Bi_2Te_3 unexpectedly develops into a Bi–Te substitutional alloy by adopting a body-centered cubic disordered structure stable at least up to 52.1 GPa. The continuously monoclinic distortion leads to the ultimate formation of the Bi–Te alloy (Fig. 5(d)), which is attributed to the Bi \rightarrow Te charge transfer under pressure. Our research demonstrates a methodology suitable for finding alloys of nonmetallic elements for a variety of applications.

4.6. Electrides

Electrides occur in various organic compounds; they have localized electrons occupying interstitial regions of the crystal structure, which behave as anions, while the ionic cores are cations [73]. In 2009, Ma and co-authors first introduced this concept to describe the transparent insulating phase of sodium at high pressure above 200 GPa [74]. We later proposed several high-pressure electrides using CALYPSO [43,75].

Lithium exhibits complex structural behavior at high pressure, which makes its structural transitions a topic of interest. Its bcc structure under ambient conditions transforms to a complex cubic $I\bar{4}3d$ structure at 42 GPa via two intermediate phases (fcc and rhombohedral $R\bar{3}m$) [76]. Above the stable pressure range of the $I\bar{4}3d$ structure (>70 GPa), experimental measurements [77–80]

suggest the existence of a semiconducting broken-symmetry phase; however, its crystal structure remains a mystery. Since then, much effort [81–84] has been devoted to the determination of this insulating phase. In 2011, we extensively explored the energy landscape of dense Li using CALYPSO, and predicted the novel semiconducting structure $\text{Aba}2\text{--}40$ (Fig. 6(a)) to be most stable at 60–80 GPa [43]. Our calculations reveal that this semiconducting electronic state emerges in the $\text{Aba}2\text{--}40$ phase owing to core exclusion and the localization of valence electrons in the voids of the crystal, which results in the formation of a new high-pressure electride similar to that in transparent Na [74]. This theoretical prediction was confirmed by independent high-pressure experiments [85] and another joint theoretical and experimental study [86].

4.7. Superconductors

Hydrogen-rich compounds are promising for high-temperature superconductors under high pressure. CALYPSO has successfully searched the superconducting high-pressure phases of hydrogen-rich compounds, including CaH_6 [87], GaH_3 [88], BeH_2 [89], NbH_2 [90], TiH_2 [91], and H_2S [92].

Hydrogen sulfide (H_2S) is a typical molecular solid [93,94] at ambient pressure. At high pressure, it transforms into three high-pressure phases [95–98] whose crystal structures are the subject of intense debate [99–104]. H_2S is not considered a superconductor as it was proposed to dissociate into its constituent elements before metallization [104]. We used CALYPSO to perform an extensive structure search on solid H_2S at pressures of 10–200 GPa. In addition to the identification of candidate structures for nonmetallic phases IV and V, two stable metallic structures with P-1 and Cmca symmetry were predicted at above 80 GPa [92] (Fig. 6(b) and (c)). The finding of these two metallic structures excludes H_2S from elemental dissociation at high pressure. Our electron–phonon coupling calculations reveal that the critical temperatures (T_c) are 60 K for the P-1 structure at 158 GPa and 82 K for the Cmca structure at 160 GPa.

Motivated by our prediction [92], a breakthrough electrical measurement indeed observed high-temperature superconductivity in compressed H_2S prepared at above 220 K; the unprecedentedly high T_c of ~ 190 K was found at 180 GPa [105]. In another sample prepared at a lower temperature of 100–150 K, the T_c of H_2S increased with pressure and reached a maximum of 150 K at 200 GPa [105], in good agreement with our predictions [92].

We also used CALYPSO to conduct an extensive structure search on calcium polyhydrides (CaH_x , $x=2\text{--}12$) at high pressure, and showed that the CaH_6 stoichiometry, which had a body-centered cubic structure with hydrogen forming unusual “sodalite” cages containing enclathrated Ca, stabilizes at above 150 GPa (Fig. 6(d)) [87]. The stability of this structure is derived from the acceptance by two H_2 of electrons donated by Ca to form an “ H_4 ” unit as the building block for the construction of the three-dimensional sodalite cage. This unique structure has a partial occupation of the degenerate orbitals at the zone center. The resultant dynamic Jahn–Teller effect helps to enhance electron–phonon coupling, and leads to the superconductivity of CaH_6 . A superconducting T_c of 220–235 K at 150 GPa obtained from the solution of the Eliashberg equations is the highest among all hydrides studied thus far [87].

4.8. Earth core materials

The extreme conditions of pressure (up to 360 GPa) and temperature (up to 6000 K) in the Earth’s core pose great challenges to replicating its environment for experimental study. An alternative (and complementary) approach is computational mineral phy-

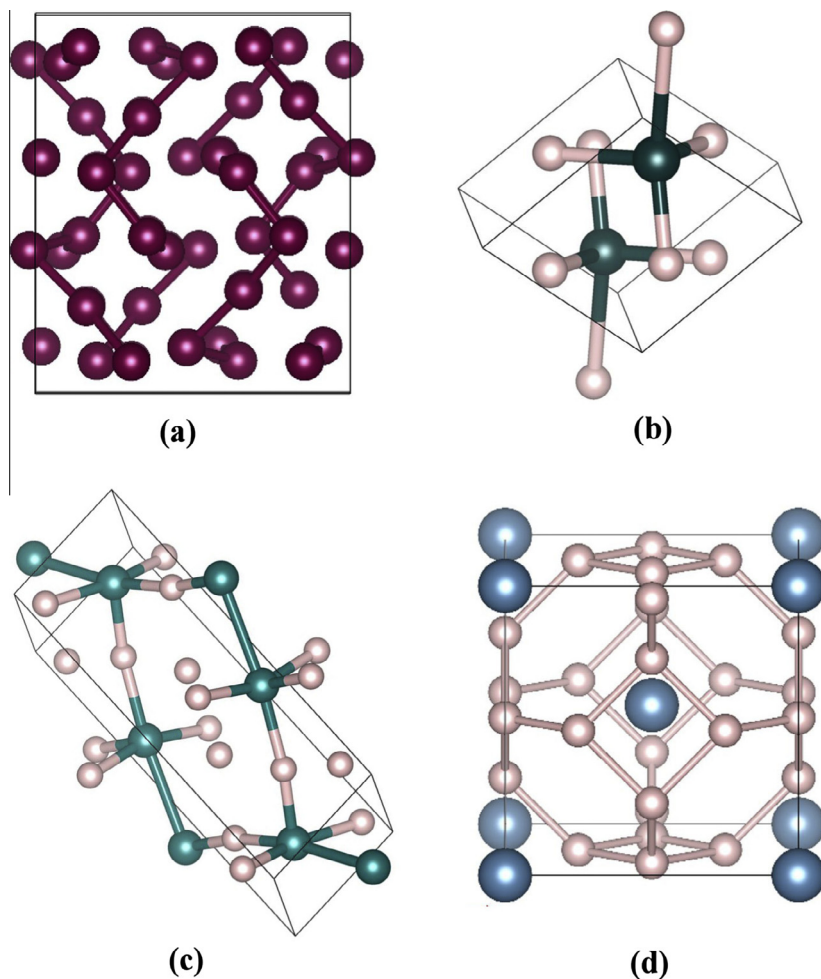


Fig. 6. The crystal structures: *Aba2*-40 of lithium (a), *P*-1 structure (b) and *Cmca* structure (c) of H_2S , (d) the bcc structure of CaH_6 .

sics, which has been widely used to improve our understanding of the Earth's core [106].

Studies of the Earth's atmosphere have shown that more than 90% of the expected amount of Xe is depleted, a finding often called the 'missing Xe paradox' [107,108]. Although several models for a Xe reservoir have been proposed, whether the missing Xe could be contained in the Earth's inner core has been under debate for a long time [109–116]. The key to addressing this issue lies in the reactivity of Xe with Fe or Ni, the main constituents of the Earth's core. We explored stable structures of XeFe_x and XeNi_x ($x = 0.25, 0.5, 1, 2, 3, 4, 5,$ and 6) compounds under the conditions of the Earth's core using CALYPSO, and calculated their formation enthalpies at 0 K and at pressures of 150, 250, and 350 GPa relative to their constituent elemental dissociation products. To estimate the effects of temperature, we also performed quasi-harmonic free-energy calculations with phonon spectra computed using the finite-displacement method. Thermal effects further stabilize the Xe–Fe/Ni compounds by lowering the formation energies of most stoichiometries. Our results show that the Earth's inner core is a natural reservoir for Xe storage, and provides a plausible solution to the missing Xe paradox.

4.9. Other materials at high pressures

High pressure can fundamentally alter the bonding patterns of elements and their compounds, leading to the unexpected

formation of materials with unusual chemical and physical properties. Using CALYPSO in combination with density functional theory calculations, we investigated the phase stabilities and structural changes of various materials under high pressure [117–128].

Chemically, the mixing of Li and B in the Li-rich regime can produce Li–B alloys with B ions in a high anionic charge state; therefore, they are ideal systems for exploring the evolution of B–B bonding features with increasing charge states of B. Unfortunately, the Li–B systems in the Li-rich regime are not stable at ambient conditions, except for $\text{LiB}_{0.88}$. Using CALYPSO in combination with density functional theory, we investigated the phase stabilities and structural changes of various Li–B systems in the Li-rich regime under high pressure [117]. We identified the formation of four stoichiometric lithium borides (Li_3B_2 , Li_2B , Li_4B , and Li_6B) having unforeseen structural features that might be experimentally synthesizable over a wide range of pressures. Strikingly, the B–B bonding patterns of these lithium borides evolve with increasing Li content from graphite-like sheets in turn to zigzag chains, dimers, and eventually isolated B ions. These intriguing B–B bonding features are chemically rationalized by the elevated B anionic charges as a result of $\text{Li} \rightarrow \text{B}$ charge transfer.

Alkali metals have long been known to possess simple electronic structures at ambient pressure that are well explained by a nearly free-electron model. However, they exhibit unexpected structures and electronic behavior at high pressures. Compression of metallic Na to 200 GPa leads to a stable wide-band-gap insulator

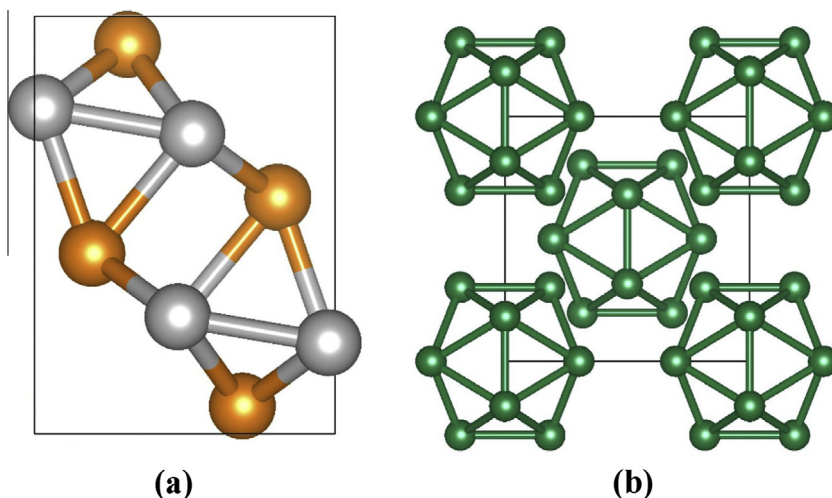


Fig. 7. The oP8 structure (a) and the cI14 structure (b) of Na.

with a double hexagonal hP4 structure [74]. The higher-pressure structures of Na remain unexplored, but they are important for investigating the pressure at which Na reverts to a metal. We reported the reversion of Na to a metal at the very high pressure of 15.5 TPa, which we predicted using CALYPSO in combination with first-principles calculations [118]. Na is therefore insulating over the large pressure range of 0.2–15.5 TPa. Unusually, Na adopts an oP8 structure at pressures of 117–125 GPa, and the same oP8 structure at 1.75–15.5 TPa (Fig. 7(a)). The metallization of Na occurs upon the formation of a stable and striking body-centered cubic cI24 electride structure (Fig. 7(b)) consisting of Na₁₂ icosahedra, each housing at its center about one electron that is not associated with any Na ion.

5. Summary

This review describes the basic theory and general features of our developed CALYPSO methodology. Its validity in predicting the structure of materials has been extensively demonstrated through its application to various materials ranging from 0D to 3D systems. We highlight a few examples of our own works applying CALYPSO to nanoclusters, diamond surfaces, superhard materials, energetic materials, electrides, superconductors, and materials of the Earth's core. These results clearly show that CALYPSO is a powerful tool for accelerating the discovery of materials. Certainly, there are still many challenging problems in the structure prediction field (e.g., high-temperature systems and large systems with more than ~100 atoms/cell), and these require the further development of structure search methods.

Acknowledgments

The authors acknowledge funding support from the National Natural Science Foundation of China (under Grants Nos. 11274136 and No. 11404128), the Postdoctoral Science Foundation of China (under Grant No. 2014M551181 and 2014M550596), Young Teacher Innovation Funding in Jilin University under Grant No. 450060501393, the Recruitment Program of Global Experts (the Thousand Young Talents Plan), 2012 Changjiang Scholar of Ministry of Education, Changjiang Scholar and Innovative Research Team in University (Grant No. IRT1132), the fund of CAEP-SCNS (R2014-03**), and the China 973 Program under Grant No. 2011CB808204.

References

- [1] F. Giustino, *Materials Modelling using Density Functional Theory: Properties and Predictions*, Oxford, 2014.
- [2] R. Yu, Q. Zhan, L.C. De Jonghe, *Angew. Chem.* 119 (2007) 1154.
- [3] C.C. Fischer, K.J. Tibbetts, D. Morgan, G. Ceder, *Nat. Mater.* 5 (2006) 641.
- [4] S. Kirkpatrick, *J. Statist. Phys.* 34 (1984) 975.
- [5] S. Brooks, B. Morgan, *Statistician* (1995) 241–257.
- [6] J.C. Schön, M. Jansen, *Angew. Chem. Int. Ed.* 35 (1996) 1286.
- [7] D. Deaven, K. Ho, *Phys. Rev. Lett.* 75 (1995) 288.
- [8] A. Kolmogorov, S. Shah, E. Margine, A. Bialon, T. Hammerschmidt, R. Drautz, *Phys. Rev. Lett.* 105 (2010) 217003.
- [9] G. Trimarchi, A. Zunger, *Phys. Rev. B* 75 (2007) 104113.
- [10] N. Abraham, M. Probert, *Phys. Rev. B* 73 (2006) 224104.
- [11] A.R. Oganov, C.W. Glass, *J. Chem. Phys.* 124 (2006) 244704.
- [12] D.C. Lonie, E. Zurek, *Comput. Phys. Commun.* 182 (2011) 372.
- [13] S. Woodley, P. Battle, J. Gale, C.A. Catlow, *Phys. Chem. Chem. Phys.* 1 (1999) 2535.
- [14] S. Goedecker, *J. Chem. Phys.* 120 (2004) 9911.
- [15] D.J. Wales, J.P. Doye, *J. Phys. Chem. A* 101 (1997) 5111.
- [16] C.J. Pickard, R. Needs, *Nat. Phys.* 3 (2007) 473.
- [17] S.M. Woodley, R. Catlow, *Nat. Mater.* 7 (2008) 937.
- [18] Y. Wang, Y. Ma, *J. Chem. Phys.* 140 (2014) 040901.
- [19] Y. Wang, J. Lv, L. Zhu, S. Lu, K. Yin, Q. Li, H. Wang, L. Zhang, Y. Ma, *J. Phys.: Condens. Matter.* 27 (2015) 203203.
- [20] C.J. Pickard, R.J. Needs, *J. Phys.: Condens. Matter.* 23 (2011) 053201.
- [21] A.R. Oganov, A.O. Lyakhov, M. Valle, *Acc. Chem. Res.* 44 (2011) 227.
- [22] Y. Wang, J. Lv, L. Zhu, Y. Ma, *Phys. Rev. B* 82 (2010) 094116.
- [23] Y. Wang, J. Lv, L. Zhu, Y. Ma, *Comput. Phys. Commun.* 183 (2012) 2063.
- [24] J. Lv, Y. Wang, L. Zhu, Y. Ma, *J. Chem. Phys.* 137 (2012) 084104.
- [25] Y. Wang, M. Miao, J. Lv, L. Zhu, K. Yin, H. Liu, Y. Ma, *J. Chem. Phys.* 137 (2012) 224108.
- [26] S. Lu, Y. Wang, H. Liu, M. Miao, Y. Ma, *Nat. Commun.* 5 (2014) 3666.
- [27] X. Zhang, Y. Wang, J. Lv, C. Zhu, Q. Li, M. Zhang, Q. Li, Y. Ma, *J. Chem. Phys.* 138 (2013) 114101.
- [28] J. Kennedy, *Particle swarm optimization*, in: *Encyclopedia of Machine Learning*, Springer, 2010, pp. 760–766.
- [29] E. Bonabeau, M. Dorigo, G. Theraulaz, *Swarm Intelligence: From Natural to Artificial Systems*, Oxford University Press, 1999.
- [30] C.O. Ourique, E.C. Biscaia Jr., J.C. Pinto, *Comput. Chem. Eng.* 26 (2002) 1783.
- [31] S.T. Call, D.Y. Zubarev, A.I. Boldyrev, *J. Comput. Chem.* 28 (2007) 1177.
- [32] P.J. Steinhardt, D.R. Nelson, M. Ronchetti, *Phys. Rev. B* 28 (1983) 784.
- [33] G. Kresse, J. Furthmüller, *Phys. Rev. B* 54 (1996) 11169.
- [34] J.M. Soler, E. Artacho, J.D. Gale, A. García, J. Junquera, P. Ordejón, D. Sánchez-Portal, *J. Phys.: Condens. Matter.* 14 (2002) 2745.
- [35] P. Giannozzi, S. Baroni, N. Bonini, M. Calandra, R. Car, C. Cavazzoni, D. Ceresoli, G.L. Chiarotti, M. Cococcioni, I. Dabo, *J. Phys.: Condens. Matter.* 21 (2009) 395502.
- [36] S.J. Clark, M.D. Segall, C.J. Pickard, P.J. Hasnip, M.I. Probert, K. Refson, M.C. Payne, *Z. Krist.* 220 (2005) 567.
- [37] J. VandeVondele, M. Krack, F. Mohamed, M. Parrinello, T. Chassaing, J. Hutter, *Comput. Phys. Commun.* 167 (2005) 103.
- [38] M.J. Frisch, G.W. Trucks, E.A. Schlegel, *Gaussian 09*, Gaussian, Inc., Wallingford, CT, USA, 2009.
- [39] B. Aradi, B. Hourahine, T. Frauenheim, *J. Phys. Chem. A* 111 (2007) 5678.
- [40] S. Plimpton, *J. Comput. Phys.* 117 (1995) 1.

- [41] J.D. Gale, *J. Chem. Soc., Faraday Trans.* 93 (1997) 629.
- [42] J. Parsons, J.B. Holmes, J.M. Rojas, J. Tsai, C.E. Strauss, *J. Comput. Chem.* 26 (2005) 1063.
- [43] J. Lv, Y. Wang, L. Zhu, Y. Ma, *Phys. Rev. Lett.* 106 (2011) 015503.
- [44] L. Zhu, H. Wang, Y. Wang, J. Lv, Y. Ma, Q. Cui, Y. Ma, G. Zou, *Phys. Rev. Lett.* 106 (2011) 145501.
- [45] J. Lv, Y. Wang, L. Zhu, Y. Ma, *Nanoscale* 6 (2014) 11692.
- [46] J. Lv, Y. Wang, L. Zhang, H. Lin, J. Zhao, Y. Ma, *Nanoscale* 7 (2015) 10482.
- [47] H.W. Kroto, J.R. Heath, S.C. O'Brien, R.F. Curl, R.E. Smalley, *Nature* 318 (1985) 162 (ISSN 0028-0836).
- [48] H.-J. Zhai, Y.-F. Zhao, W.-L. Li, Q. Chen, H. Bai, H.-S. Hu, Z.A. Piazza, W.-J. Tian, H.-G. Lu, Y.-B. Wu, Y.-W. Mu, G.-F. Wei, Z.-P. Liu, J. Li, S.-D. Li, L.S. Wang, *Nat. Chem.* 6 (2014) 727.
- [49] Q. Chen, W.-L. Li, Y.-F. Zhao, S.-Y. Zhang, H.-S. Hu, H. Bai, H.-R. Li, W.-J. Tian, H.-G. Lu, H.-J. Zhai, S.-D. Li, J. Li, L.S. Wang, *ACS Nano* 9 (2015) 754.
- [50] Y. Chai, T. Guo, C. Jin, R.E. Haufler, Chibante, L.P. Felipe, J. Fure, L. Wang, J.M. Alford, R.E. Smalley, *J. Phys. Chem.* 95 (1991) 7564.
- [51] H. Hiura, T. Miyazaki, T. Kanayama, *Phys. Rev. Lett.* 86 (2001) 1733.
- [52] V. Kumar, Y. Kawazoe, *Phys. Rev. Lett.* 87 (2001) 045503.
- [53] S.N. Khanna, B.K. Rao, P. Jena, *Phys. Rev. Lett.* 89 (2002) 016803.
- [54] F. Bechstedt, A. Stekolnikov, J. Furthmüller, P. Käckell, *Phys. Rev. Lett.* 87 (2001) 016103.
- [55] B. Bonanni, G. Bussetti, A. Violante, P. Chiaradia, C. Goletti, *J. Phys.: Condens. Matter.* 25 (2013) 485008.
- [56] A. Stekolnikov, J. Furthmüller, F. Bechstedt, *Phys. Rev. B* 65 (2002) 115318.
- [57] F. Celii, J. Butler, *Annu. Rev. Phys. Chem.* 42 (1991) 643.
- [58] M. Zhang, H. Liu, Q. Li, B. Gao, Y. Wang, H. Li, C. Chen, Y. Ma, *Phys. Rev. Lett.* 114 (2015) 015502.
- [59] Q. Li, D. Zhou, W. Zheng, Y. Ma, C. Chen, *Phys. Rev. Lett.* 110 (2013) 136403.
- [60] Q. Li, J. Wang, M. Zhang, Q. Li, Y. Ma, *RSC Adv.* 5 (2015) 35882.
- [61] Q. Li, H. Liu, D. Zhou, W. Zheng, Z. Wu, Y. Ma, *Phys. Chem. Chem. Phys.* 14 (2012) 13081.
- [62] Y. Li, Q. Li, Y. Ma, *Europhys. Lett.* 95 (2011) 66006.
- [63] H. Liu, Q. Li, L. Zhu, Y. Ma, *Solid State Commun.* 115 (2011) 716.
- [64] P. Zinin, L. Ming, H. Ishii, R. Jia, T. Acosta, E. Hellebrand, *J. Appl. Phys.* 111 (2012) 114905.
- [65] M.J. Lipp, W.J. Evans, B.J. Baer, C.S. Yoo, *Nat. Mater.* 4 (2005) 211.
- [66] M.I. Eremets, A.G. Gavriliuk, I.A. Trojan, D.A. Dzivenko, R. Boehler, *Nat. Mater.* 3 (2004) 558.
- [67] W.J. Evans, M.J. Lipp, C.-S. Yoo, H. Cynn, J.L. Herberg, R.S. Maxwell, M.F. Nicol, *Chem. Mater.* 18 (2006) 2520.
- [68] X. Wang, Y. Wang, M. Miao, X. Zhong, J. Lv, T. Cui, J. Li, L. Chen, C.J. Pickard, Y. Ma, *Phys. Rev. Lett.* 109 (2012) 175502.
- [69] K. Yin, Y. Wang, H. Liu, F. Peng, L. Zhang, *J. Mater. Chem. A* 3 (2015) 4188.
- [70] C. Zhu, Q. Li, Y. Zhou, M. Zhang, S. Zhang, Li, *J. Phys. Chem. C* 118 (2014) 27252.
- [71] G. Wang, T. Cagin, *Appl. Phys. Lett.* 89 (2006) 152101.
- [72] J.L. Zhang et al., *Proc. Natl. Acad. Sci. U.S.A.* 108 (2010) 24.
- [73] D. Issa, J.L. Dye, *J. Am. Chem. Soc.* 104 (1982) 3781.
- [74] Y. Ma, M. Eremets, A.R. Oganov, Y. Xie, I. Trojan, S. Medvedev, A.O. Lyakhov, M. Valle, V. Prakapenka, *Nature* 458 (2009) 182.
- [75] P. Li, G. Gao, Y. Wang, Y. Ma, *J. Phys. Chem. C* 114 (2010) 21745.
- [76] M. Hanfland, K. Syassen, N. Christensen, D. Novikov, *Nature* 408 (2000) 174.
- [77] A.F. Goncharov, V.V. Struzhkin, H.-K. Mao, R.J. Hemley, *Phys. Rev. B* 71 (2005) 184114.
- [78] V.V. Struzhkin, M.I. Eremets, W. Gan, H.-K. Mao, R.J. Hemley, *Science* 298 (2002) 1213.
- [79] S. Deemyad, J.S. Schilling, *Phys. Rev. Lett.* 91 (2003) 167001.
- [80] T. Matsuoka, S. Onoda, M. Kaneshige, Y. Nakamoto, K. Shimizu, T. Kagayama, Y. Ohishi, *J. Phys.: Conference Series*, IOP Publishing, 2008.
- [81] J. Neaton, N. Ashcroft, *Nature* 400 (1999) 141.
- [82] Y. Ma, A.R. Oganov, Y. Xie, *Phys. Rev. B* 78 (2008) 014102.
- [83] C.J. Pickard, R. Needs, *Phys. Rev. Lett.* 102 (2009) 146401.
- [84] Y. Yao, S.T. John, D.D. Klug, *Phys. Rev. Lett.* 102 (2009) 115503.
- [85] C.L. Guillaume, E. Gregoryanz, O. Degtyareva, M.I. McMahon, M. Hanfland, S. Evans, M. Guthrie, S.V. Sinogeikin, H. Mao, *Nat. Phys.* 7 (2011) 211.
- [86] M. Marqués, M. McMahon, E. Gregoryanz, M. Hanfland, C. Guillaume, C. Pickard, G. Ackland, R. Nelves, *Phys. Rev. Lett.* 106 (2011) 095502.
- [87] H. Wang, S.T. John, K. Tanaka, T. Iitaka, Y. Ma, *Proc. Natl. Acad. Sci. U.S.A.* 109 (2012) 6463.
- [88] G. Gao, H. Wang, A. Bergara, Y. Li, G. Liu, Y. Ma, *Phys. Rev. B* 84 (2011) 064118.
- [89] Z. Wang, Y. Yao, L. Zhu, H. Liu, T. Iitaka, H. Wang, Y. Ma, *J. Chem. Phys.* 140 (2014) 124707.
- [90] G. Gao, R. Hoffmann, N.W. Ashcroft, H. Liu, A. Bergara, Y. Ma, *Phys. Rev. B* 88 (2013) 184104.
- [91] G. Gao, A. Bergara, G. Liu, Y. Ma, *J. Appl. Phys.* 113 (2013) 103512.
- [92] Y. Li, J. Hao, H. Liu, Y. Li, Y. Ma, *J. Chem. Phys.* 140 (2014) 174712.
- [93] M. Collins, C. Ratcliffe, J. Ripmeester, *J. Phys. Chem.* 93 (1989) 7495.
- [94] J.K. Cockcroft, A.N. Fitch, Z. Krist. 193 (1990) 1.
- [95] H. Shimizu, Y. Nakamichi, S. Sasaki, *J. Chem. Phys.* 95 (1991) 2036.
- [96] S. Endo, N. Ichimiya, K. Koto, S. Sasaki, H. Shimizu, *Phys. Rev. B* 50 (1994) 5865.
- [97] S. Endo, A. Honda, S. Sasaki, H. Shimizu, O. Shimomura, T. Kikegawa, *Phys. Rev. B* 54 (1996) R717.
- [98] M. Sakashita, H. Yamawaki, H. Fujihisa, K. Aoki, S. Sasaki, H. Shimizu, *Phys. Rev. Lett.* 79 (1997) 1082.
- [99] H. Fujihisa, H. Yamawaki, M. Sakashita, K. Aoki, S. Sasaki, H. Shimizu, *Phys. Rev. B* 57 (1998) 2651.
- [100] S. Endo, A. Honda, K. Koto, O. Shimomura, T. Kikegawa, N. Hamaya, *Phys. Rev. B* 57 (1998) 5699.
- [101] R. Rousseau, M. Boero, M. Bernasconi, M. Parrinello, K. Terakura, *Phys. Rev. Lett.* 83 (1999) 2218.
- [102] T. Ikeda, *Phys. Rev. B* 64 (2001) 104103.
- [103] L. Wang, F. Tian, W. Feng, C. Chen, Z. He, Y. Ma, T. Cui, B. Liu, G. Zou, *J. Chem. Phys.* 132 (2010) 164506.
- [104] R. Rousseau, M. Boero, M. Bernasconi, M. Parrinello, K. Terakura, *Phys. Rev. Lett.* 85 (2000) 1254.
- [105] A. Drozdov, M. Eremets, I. Troyan (2014), arXiv:1412.0460.
- [106] Lidunka Voadlo, *New Views of the Earth's Inner Core from Computational Mineral Physics*, in: *New Frontiers in Integrated Solid Earth Sciences*, SpringerScience+Business Media, B.V., 2010.
- [107] E. Anders, T. Owen, *Science* 198 (1977) 453.
- [108] R.O. Pepin, D. Porcelli, *Rev. Min. Geochem.* 47 (2002) 191.
- [109] G.T. Sill, L.L. Wilkening, *Icarus* 33 (1978) 13.
- [110] J.F. Wacker, E. Anders, *Geochim. Cosmochim. Acta* 48 (1984) 2373.
- [111] J.-I. Matsuda, K. Matsubara, *Geophys. Res. Lett.* 16 (1989) 81.
- [112] W.A. Caldwell, J.H. Nguyen, B.G. Pfrommer, F. Mauri, S.G. Louie, R. Jeanloz, *Science* 277 (1997) 930.
- [113] A.P. Jephcoat, *Nature* 393 (1998) 355.
- [114] C. Sanloup, B.C. Schmidt, E.M.C. Perez, A. Jambon, E. Gregoryanz, M. Mezour, *Science* 310 (2005) 1174.
- [115] K.K.M. Lee, G. Steinle-Neumann, *J. Geophys. Res.* 111 (2006) B02202.
- [116] D. Nishio-Hamane, T. Yagi, N. Sata, T. Fujita, T. Okada, *Geophys. Res. Lett.* 37 (2010) L04302.
- [117] F. Peng, M. Miao, H. Wang, Q. Li, Y. Ma, *J. Am. Chem. Soc.* 134 (2012) 18699.
- [118] Y. Li, Y. Wang, C.J. Pickard, R.J. Needs, Yi Wang, Y. Ma, *Phys. Rev. Lett.* 114 (2015) 125501.
- [119] L. Zhu, Z. Wang, Y. Wang, G. Zou, H.K. Mao, Y. Ma, *Proc. Natl. Acad. Sci. USA* 109 (2012) 751.
- [120] C. Lu, M. Miao, Y. Ma, *J. Am. Chem. Soc.* 135 (2013) 14167.
- [121] X. Zhong, Y. Wang, F. Peng, H. Liu, H. Wang, Y. Ma, *Chem. Sci.* 5 (2014) 3936.
- [122] Z. Wang, H. Wang, J.S. Tse, T. Iitaka, Y. Ma, *Chem. Sci.* 6 (2015) 522.
- [123] S. Wei, C. Zhu, Q. Li, Y. Zhou, Q. Li, Y. Ma, *Phys. Chem. Chem. Phys.* 16 (2014) 17924.
- [124] Y. Chen, X. Xi, W. Yim, F. Peng, Y. Wang, H. Wang, Y. Ma, G. Liu, C. Sun, C. Ma, Z. Chen, H. Berger, *J. Phys. Chem. C* 117 (2013) 25677.
- [125] Y. Chen, F. Peng, Y. Yan, Z. Wang, C. Sun, Y. Ma, *J. Phys. Chem. C* 117 (2013) 13879.
- [126] X. Chen, Y. Ma, *Europhys. Lett.* 100 (2012) 26005.
- [127] H. Liu, H. Wang, Y. Ma, *J. Phys. Chem. C* 116 (2012) 9221.
- [128] Y. Wang, H. Liu, J. Lv, L. Zhu, H. Wang, Y. Ma, *Nat. Commun.* 2 (2011) 563.